Vocal fold vibration mode changes due to cricothyroid and thyroarytenoid muscle interaction in a three-dimensional model of the canine larynx

Biao Geng, Mohammadreza Movahhedi, Qian Xue, et al.

Citation: The Journal of the Acoustical Society of America 150, 1176 (2021); doi: 10.1121/10.0005883

View online: https://doi.org/10.1121/10.0005883

View Table of Contents: https://asa.scitation.org/toc/jas/150/2

Published by the Acoustical Society of America

ARTICLES YOU MAY BE INTERESTED IN

Effects of cricothyroid and thyroarytenoid interaction on voice control: Muscle activity, vocal fold biomechanics, flow, and acoustics

The Journal of the Acoustical Society of America 150, 29 (2021); https://doi.org/10.1121/10.0005275

Visual feedback of the tongue influences speech adaptation to a physical modification of the oral cavity The Journal of the Acoustical Society of America **150**, 718 (2021); https://doi.org/10.1121/10.0005520

Vocal fold dynamics in a synthetic self-oscillating model: Intraglottal aerodynamic pressure and energy The Journal of the Acoustical Society of America **150**, 1332 (2021); https://doi.org/10.1121/10.0005882

Mandarin tone recognition training with cochlear implant simulation: Amplitude envelope enhancement and cue weighting

The Journal of the Acoustical Society of America 150, 1218 (2021); https://doi.org/10.1121/10.0005878

Examining vocal attractiveness through articulatory working space

The Journal of the Acoustical Society of America 150, 1548 (2021); https://doi.org/10.1121/10.0005730

Modelling microprosodic effects can lead to an audible improvement in articulatory synthesis The Journal of the Acoustical Society of America **150**, 1209 (2021); https://doi.org/10.1121/10.0005876







Vocal fold vibration mode changes due to cricothyroid and thyroarytenoid muscle interaction in a three-dimensional model of the canine larynx

Biao Geng, Mohammadreza Movahhedi, Qian Xue, a) and Xudong Zhengb) Department of Mechanical Engineering, University of Maine, Orono, Maine 04473, USA

ABSTRACT:

Using a continuum model based on magnetic resonance imaging of a canine larynx, parametric simulations of the vocal fold vibration during phonation were conducted with the cricothyroid muscle (CT) and the thyroarytenoid muscle (TA) independently activated from zero to full activation. The fundamental frequency (f_0) first increased and then experienced a downward jump as TA activity gradually increased under moderate to high CT activation. Proper orthogonal decomposition analysis revealed that the vocal fold vibrations were dominated by two modes representing a lateral motion and rotational motion, respectively, and the f_0 drop was associated with a switch on the order of the two modes. In another parametric set where only the vocalis was active, f_0 increased monotonically with both TA and CT activity and the mode switch did not occur. The results suggested that the active stress in the TA, which causes large stress differences between the body and cover, is essential for the occurrence of the rotational mode and mode switch. Relatively greater TA activity tends to promote the rotational mode, while relatively greater CT activity tends to promote the lateral mode. The results also suggested that the vibration modes affected f_0 by affecting the contribution of the TA stress to the effective stiffness. The switch in the dominant mode caused the non-monotonic change of f_0 . © 2021 Acoustical Society of America. https://doi.org/10.1121/10.0005883

(Received 3 November 2020; revised 19 July 2021; accepted 26 July 2021; published online 16 August 2021)

[Editor: Zhaoyan Zhang] Pages: 1176–1187

I. INTRODUCTION

The role of the thyroarytenoid muscle (TA) in frequency regulation has been known to be complex. It has been widely accepted that TA activation could either raise or lower the fundamental frequency (f_0) depending on the state of the vocal folds. 1-3 However, it is still not fully clear under what conditions TA activity would raise or lower f_0 and the mechanisms behind it. Based on in vivo electromyography (EMG) measures and thyroarytenoid stimulation on human subjects, Titze et al. suggested that "at lower fundamental frequencies and lower vocal intensities, f_0 correlates positively with TA activity, but at higher fundamental frequencies and low intensity (especially in falsetto voice) an increase in TA tends to lower f_0 ." This indicates that TA activation would lower f_0 under high cricothyroid muscle (CT) activation and increase it under low CT activation. Yin and Zhang² studied the eigenfrequencies of vocal fold vibration in the full CT vs TA space using pre-stressed eigenanalysis on a simplified continuum vocal fold model with muscle activation. They found that TA always lowered the eigenfrequencies under high CT activation; under low CT activation, TA first lowered and then increased the eigenfrequencies; the eigenfrequencies increased monotonically with TA activation only when CT was not activated. However, a more recent in vivo study using graded muscle

b)ORCID: 0000-0001-5403-8862.

stimulation on a canine model³ showed an opposite trend that "across all CT and LCA/IA conditions..., an increase in TA activity always first raised f_0 and then lowered f_0 " (see Fig. 8 in Chhetri $et\ al.^3$). One possible cause of the opposite trends found in the eigenanalysis and $in\ vivo$ investigation might be that the eigenfrequency of a single mode was not representative of the fundamental frequency because the flow-structure interaction (FSI) involves entrainment of multiple modes.

In addition to its role in frequency control, TA is also widely believed to be important in regulating vocal registers. A very popular point of view is to regard the modal/chest register as TA-dominant and the falsetto/head register as CT-dominant (see, e.g., Ref. 4), following perhaps the studies by Hirano using EMG.⁵ However, more recent EMG studies^{6,7} are not in support of this, as it was found that CT was dominant for most of the frequency range even in the chest register.

The vocal registers are thought to be associated with different vibratory mechanisms as is shown from electroglottograph (EGG) signals and the sound spectrum. However, when observed using videokymography and strobo-laryngoscopy, the basic surface vibration pattern has been reported to share the same features across different registers, for example, vibration along the whole glottal length and vertical phase difference. Hirano proposed four types of vocal fold configurations/vibration modes under CT and TA interaction based on the body-cover structure of the

a)Electronic mail: qian.xue@maine.edu

vocal fold tissue composition to illustrate the vibratory mechanisms corresponding to different registers. However, these vibration modes remained largely hypothetical, as it is difficult to measure the internal kinematics of the vocal fold in experiments and previous numerical simulations of vocal fold vibration did not include the muscle mechanics. Some investigations that embedded trackers inside the vocal folds to reveal the internal motion showed that the vibration amplitude decreases deep into the vocal folds as muscle activity increases, but no information regarding vibrational modes was available. Moreover, Hirano's description of the laryngeal adjustments was largely qualitative, and it is not clear when these vibration modes transition to each other under muscle activities.

The frequency change within the same register/laryngeal mechanism is believed to be smooth with gradual variation of muscle activity, and the transitions between registers are usually accompanied by a frequency jump. ¹² Previous experimental studies showed that frequency jumps could occur with ^{3,13} or without ¹² TA activity.

The objective of this study is to use a computational laryngeal model that incorporates laryngeal muscle mechanics to investigate the role of CT and TA interaction in frequency regulation during voice production as well as the underlying mechanism of vocal fold vibration causing the frequency change. The computer model includes the major links in the process of voice production, making it possible to investigate the cause-effect relationship between muscle activity and the vocal fold vibration by detailed investigation of the movements of the internal vocal fold tissues. Proper orthogonal decomposition (POD) was used to analyze the vocal fold vibration from current simulations. The same method has been widely used since its first application by Berry *et al.* ¹⁴ to interpret high-order biomechanical simulations of normal and chaotic vocal fold oscillations.

II. METHODS

A. Simulation setup

The current simulations were based on a muscle activation model and a three-dimensional (3D) larynx model that were developed previously. Readers are referred to the previous work¹⁵ for a more detailed description of the reconstruction of the laryngeal components from magnetic resonance imaging (MRI) data. Briefly, a full larynx model [Fig. 1(a)] was constructed from MRI data of a dissected canine larynx, which included all relevant laryngeal cartilages and intrinsic laryngeal muscles. The cricoarytenoid joint (CAJ), which is essential in modeling vocal fold posturing, was modeled as a rotating-sliding motion, which allowed the arytenoid cartilages to move with two degrees of freedom: a linear movement along the long joint axis and a rotational movement around the long joint axis. It was implemented by constraining the two vertices of the arytenoid facet of the CAJ to the axis (long joint axis) defined by these two vertices. It was shown previously that such simplification of the joint motion was able to predict a wide range of posturing maneuvers with correct vocal fold movements. 15 The muscle activation was modeled using the Hillbased contractile element, 16,17 in which the uniaxial active muscle stress was proportional to the maximum active stress and the muscle activation level and was calculated in the fiber direction defined by the origin and insertion points of a muscle bundle. For completeness, a detailed description of the muscle model is included in the Appendix.

The vocal fold vibration was simulated using a twostage approach to reduce the computational cost. In the first stage, static vocal fold posturing under specific muscle activations was simulated on the full larynx model. The displacements of the vocal fold boundary areas connecting the cartilages and adjacent areas [see the black dots in Fig. 1(b)] were then extracted from the solution. In the second stage, dynamic simulation of FSI was performed using the left vocal fold only [Fig. 1(b)] with the same tissue composition [shown in Fig. 1(c)], including the paraglottic space (PGS), the cover layer, the conus elasticus (CE), the thyroarytenoid vocalis muscle (TAv), the thyroarytenoid muscularis muscle (TAm), and the lateral cricoarytenoid muscle (LCA). The same material parameters as in the previous work 15 were used for the muscles (see also the Appendix). For nonmuscle tissues, (nearly) incompressible Mooney-Rivlin materials were used. The parameters were fitted to have equivalent stiffness to the materials used previously 15 under small strain and are listed in Table I. The displacements

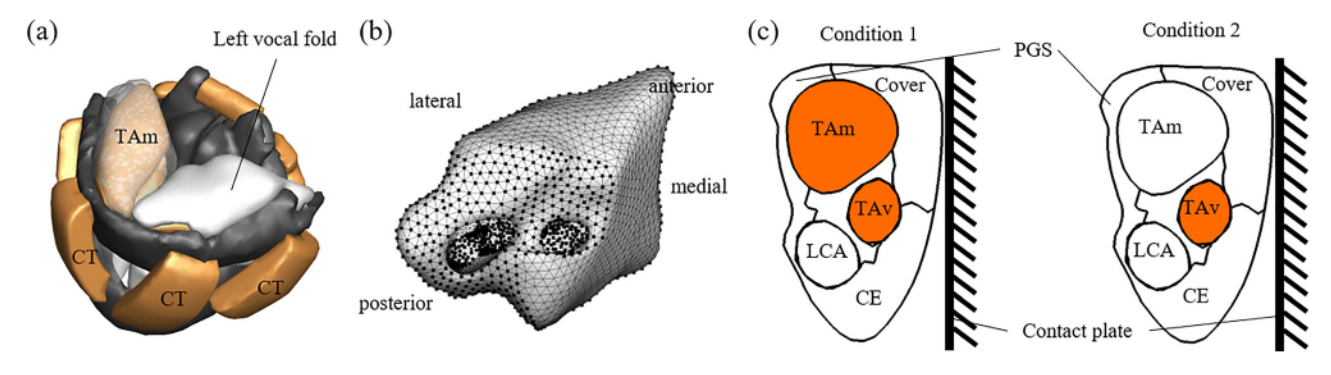


FIG. 1. (Color online) (a) Full larynx model in neutral position. The right vocal fold is made transparent to show the thyromuscularis. (b) Left vocal fold. Black dots denote boundary nodes with prescribed displacements. (c) Parametric simulation setup. In the first parametric set (condition 1), both the TAv and the TAm bundles of the TA were active. In the second parametric set (condition 2), only the TAv was active.

TABLE I. Material parameters for non-muscle tissues.

Tissue	C ₁₀ (kPa)	C ₀₁ (kPa)
Cover	0.117	0.295
PGS (adipose)	0.117	0.295
CE	2.000	1.500
Inter-muscular tissue	0.117	0.295

extracted in the first stage were used as prescribed boundary conditions for the boundary nodes [black dots in Fig. 1(b)]. The TAs were activated accordingly. In this way, the prephonatory posture and tension under a muscle condition were generated. Note that in the current study, the stress-free neutral posture (without any muscle activation) of the vocal fold is in the adducted position (no vocal process gap) based on the MRI scan. Activation of CT and TA only changed the elongation and bulging of the vocal fold.

The vocal fold model was coupled with a onedimensional (1D) Bernoulli flow model to simulate the FSI between the vocal fold and glottal flow. Previous comparison 18 between the Navier–Stokes model and Bernoulli model for the glottal flow showed that the Bernoulli flow model was adequate for obtaining reasonable predictions in terms of displacement and qualitative vocal fold vibration. It is favorable in the current study because its low computational cost makes parametric simulations possible. The flow was assumed to separate at the minimum glottal area. Downstream of the separation point, the pressure was assumed to equal the supraglottal pressure, which was assumed to be zero. Upstream of the separation point, the pressure was solved using the Bernoulli equation without considering the viscous loss,

$$p(y) = p_{sub} - \frac{1}{2} \rho_{air} \left(\frac{Q}{A(y)}\right)^2, \tag{1}$$

where p(y) is the intraglottal pressure at the location y, A(y) is the cross-sectional area at this location, p_{sub} is the subglottal pressure, Q is the air flow rate, and ρ_{air} is the density of air. The flow rate is a passive outcome from the FSI and was calculated as

$$Q = \sqrt{\frac{2p_{sub}}{\rho_{air}}} A_{min}, \tag{2}$$

where A_{min} is the minimum cross-sectional area along the glottal channel, which is also the cross-sectional area of the glottis at the flow separation point. In this study, a constant subglottal pressure of 2 kPa was used for all the cases. This was determined based on a previous *in vivo* canine model study³ that showed a maximum onset subglottal pressure of about 2 kPa across the full range of intrinsic laryngeal muscle activity.

A contact plate was set up to simulate vocal fold contact, which was modelled using a penalty-based face-toface contact model. A penalty pressure was applied to the face elements that cross the midline. The penalty pressure was specified as a linear function of the over-closure as $p_{\text{contact}} = K_c \Delta X$, where $K_c = 1000 \,\text{kPa}$ is the spring constant and ΔX is the over-closure. The resultant contact pressure for the parametric simulations was in the range of 2–7 kPa, which is comparable to values from previous experimental results.¹⁹

Two sets of parametric simulations were conducted. The difference between the two sets of simulations is illustrated in Fig. 1(c). In the first parametric set (condition 1), both the TAv and the TAm bundles of the TA were active. In the second parametric set (condition 2), only the TAv was active. The simulation was run for 0.2 s. All simulated cases either had reached nearly steady-state sustained vibration or were damped out after 0.1 s. The mean flow rate was in the range of 300–1200 ml/s. For analysis, data for the last 0.1 s were used to exclude transient effects.

The cases in a parametric set are referred to by the activation levels (a_{CT} , a_{TA}), where both a_{CT} and a_{TA} are in the range of [0, 100%]. For example, case (0.5, 0.4) is the case in which the activation of CT is 50% and TA 40%. Cases (*, 0.4) include all the cases with the same TA level of 40% and CT levels from 0 to 1.

B. POD analysis

To analyze the vocal fold dynamics, we performed POD on the vocal fold vibration. POD is a classic method of data analysis aimed at obtaining low-dimensional approximate descriptions of high-dimensional dynamic processes. For the POD analysis, the 3D motion history of the vocal fold vibration is taken as the input. The output is the decomposed base modes (POD modes) of the vibration and their corresponding amplitude coefficients (which vary periodically with time for cases with sustained vibration). The motion history is a superposition of the POD modes scaled with the amplitude coefficients. Compared to the eigenanalysis, the POD shows what vibration modes are actually triggered in the dynamic process.

Mathematically, the decomposition of a vocal fold vibration into POD modes can be expressed as

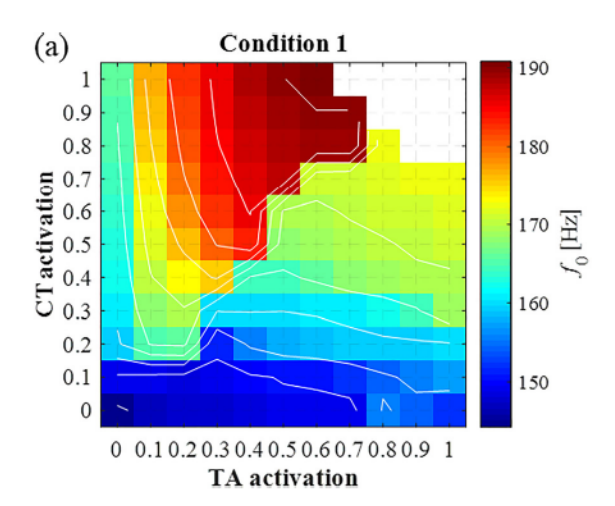
$$x(\mathbf{X}, t) = \mathbf{M}_0(\mathbf{X}) + C_1(t)\mathbf{M}_1(\mathbf{X}) + C_2(t)\mathbf{M}_2(\mathbf{X}) + \cdots,$$
 (3)

where x is the three-dimensional displacement as a function of node coordinates \mathbf{X} and time t, \mathbf{M} is the POD mode, and C is the mode amplitude coefficient. \mathbf{M}_0 is the mean deformation, which can be regarded as the equilibrium position. The POD modes are sorted in descending order by their energy proportion, i.e., the lower modes are more dominant. For the algorithm used to compute the POD modes, a brief description is available in Refs. 14 and 21. The POD modes are mutually orthogonal, i.e., the dot product of any two POD modes derived from the same motion is zero.

III. RESULTS

A. f₀ variation under CT and TA interaction

Figure 2 shows the fundamental frequency variation under CT and TA interaction when both the TAv and TAm



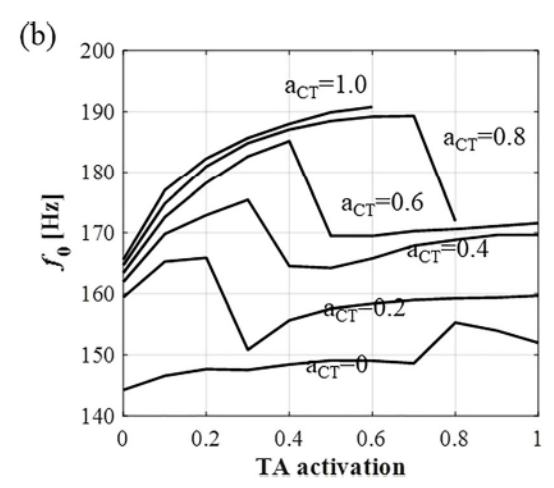


FIG. 2. (Color online) Fundamental frequency variation under CT and TA interaction when both TAv and TAm were active (condition 1). (a) Contour plot. (b) Line plots at different CT levels.

were active (condition 1). Figure 2(a) is a contour plot, while Fig. 2(b) is a line plot with selected CT levels for the same data to better illustrate the changes in values. In this parametric set, f_0 varied in the range of about 145 Hz at (0, 0) to 190 Hz at (0.6, 1.0), which accounts for about four and a half semitones. This range of frequency is small compared to that of a normal human or what was reported in *in vivo* canine experiments $(69-772 \, \text{Hz})$. This could be due to the uncertainties in material properties in the current model. The fixed subglottal pressure $(2 \, \text{kPa})$ and the limited vocal fold stretch in current simulations may also have contributed to the small range of f_0 .

From the contour plot in Fig. 2, CT activation always increased f_0 regardless of the TA activation level, and a discontinuous jump of f_0 occurred when CT activation was beyond a certain level. The activation level of CT at which the f_0 jump occurred increased with TA activity. The variation of f_0 with TA activity showed a more complex pattern. For very low CT activations ($a_{CT} \le 0.1$), f_0 remained low despite TA activity. Only a slight rise was seen as TA reached full activation. For other CT activation levels (0.2-0.8), f_0 first increased with TA activity and then underwent a significant drop, after which it increased again but to a much smaller extent. The three-phase non-monotonic trend of f_0 was similar under different CT levels with the differences only in the values of f_0 and the TA levels at which the transition occurred: as the CT level became higher, the drop of f_0 also occurred at higher TA levels. The highest possible f_0 occurred at full CT activation and medium (0.5–0.6) TA activation. A similar first-increase-then-drop trend of f_0 was also observed in an in vivo experiment. In the experiment, under high CT activations, f_0 saw a slight decrease after the peak value before the sudden drop. This phenomenon was not observed in the current simulation.

B. Vibration analysis and transition of POD modes

From our current understanding of voice production, the gradual change of f_0 with CT and TA activation is

produced within the same vibratory mode, while the sudden f_0 change is associated with transition of the vibratory mode from one to another. Such understanding is largely based on reports of changes in voice spectrum and EGG signal associated with frequency jumps. With the current model, it is possible to investigate the motion of the internal tissues under muscle activities and directly link the f_0 change and vibratory mechanisms.

To quantify the change of vibratory patterns, the vocal fold vibration was decomposed into 10 POD modes, which was enough to accurately reconstruct the original motion. The square of the amplitude of the modal coefficients can be regarded as the modal energy. The total energy of the vocal fold vibration was calculated as the summation of the modal energy. The POD analysis revealed that the first two modes made up a large proportion of the total energy for all the cases. M1, which was the most dominant mode, made up about 50%–75% of the total energy across all the cases. M2, which was the second most dominant mode, made up about 20%-40% of the total energy across all the cases. The total energy percentage of M1 and M2 is plotted in Fig. 3. For the majority of cases ($a_{CT} \ge 0.4$), M1 and M2 made up more than 90% of the total energy. Even in the lower region (right bottom corner of Fig. 3), M1 and M2 together made up more than 75% of the total energy. The modes M1 and M2 were a pair, both of which had the same frequency as f_0 . The higher POD modes were found to have the frequencies of higher harmonics of f_0 . Therefore, M1 and M2 are the focus of the current investigation.

The mode shapes of M1 and M2 changed with CT and TA activation levels, but the detailed 3D structure of the deformation is hard to present for all the cases. Taking the (0.5, 0.4) and (0.5, 0.5) as examples, the mode shapes of M1 and M2 are plotted in Fig. 4. These two cases are chosen to illustrate changes in POD modes over the frequency drop. It will be shown later that other cases before and after the frequency drop had similar mode shapes to those of the two cases illustrated. The vectors (red lines) show the normalized displacements on the deformed shape. Note that the

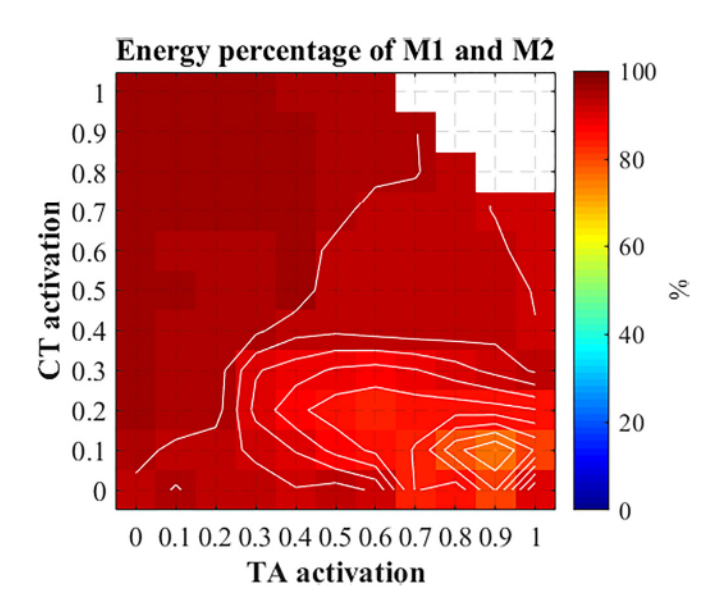


FIG. 3. (Color online) Total energy percentage of vocal fold vibration mode, M1 and M2, based on POD of vocal fold vibration in condition 1.

vector length is not representative of actual magnitude. Annotational arrows (black) are used to better illustrate the pattern.

M1s of cases (0.5, 0.4) and (0.5, 0.5) show two distinct motion patterns. In M1 of (0.5, 0.4), around the medial part of the cover layer, the lateral component of the displacement is dominant. The displacement in the TAm shows a divergent pattern in which the superior portion moves laterally and upward while the inferior portion moves laterally and downward. The subglottal portion of the vocal fold (including the TAv and the CE) also moves downward. The amplitude of the displacement vector decreases deep into the TAm. The superior part of the cover also has very small

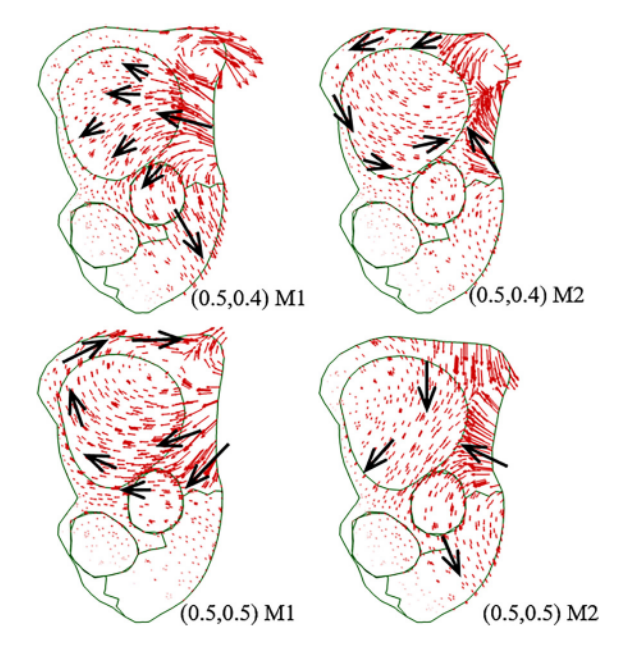


FIG. 4. (Color online) Displacement vectors of M1 and M2 for cases (0.5, 0.4) and (0.5, 0.5). Vector length (red lines) is not representative of actual magnitude. Black arrows indicate local movement direction.

displacement. In M1 of (0.5, 0.5), the displacement in the medial portion of the cover layer has a significant downward vertical component. The displacement vector is almost tangent to the medial-inferior boundary of the TAm. The displacement in the TAm undergoes a continuous change in direction from lateral at the inferior aspect to upward at the lateral part. Together with the medial-ward movement of the superior part of the cover layer, it forms a circular pattern of motion around a virtual center at the superior-medial boundary of the TAm muscle. Deep into the TAm, the amplitude of the displacement vector does not decrease as much as in the case (0.5, 0.4). The subglottal part of the vocal fold has a noticeably smaller amplitude of motion compared to that in (0.5, 0.4).

M2s of the two cases are also distinct. Interestingly, they both have some similar features to those in M1 described above. For example, M2 of case (0.5, 0.4) also shows a circular motion pattern in the vocal fold at the glottis level like that in M1 in (0.5, 0.5). Specifically, the medial cover moves laterally and upward, while the superior cover moves laterally with the horizontal component being dominant. It is interesting to note that the direction of the rotation of the TAm is different in M2 of (0.5, 0.4) and M1 of (0.5, 0.5). This M2 also has a smaller magnitude of motion in the subglottic region like M1 in (0.5, 0.5). M2 of case (0.5, 0.5) shows a dominant lateral component in the medial portion of the cover layer and a larger magnitude of motion in the subglottic region, like M1 in (0.5, 0.4). These crosssimilarities between the two modes indicate that there was likely a mode order switch underlying the change of vibration pattern across the frequency drop.

To quantify the POD mode change, mode similarity (denoted as π) is calculated for the full CT vs TA space. The similarity is quantified by the dot product of two POD modes (represented as normalized vectors). Please note that because CT activation slightly changes the mode shape, it is more consistent to use a case with the same CT activation as the baseline case to quantify the effect of TA activation on mode order switch. In our calculations, the $a_{TA} = 0.1$ case was used as the baseline case for each CT activation level. Mathematically, the similarity of the *n*th POD mode of a case (a_{CT} , a_{TA}) to the *m*th POD mode of the baseline case (a_{CT} , 0.1) is calculated as

$$\pi_{\text{nm}}(a_{\text{CT}}, a_{\text{TA}}) = |\mathbf{M}_{\text{n}}(a_{\text{CT}}, a_{\text{TA}}) \cdot \mathbf{M}_{\text{m}}(a_{\text{CT}}, 0.1)|,$$
(4)

where \mathbf{M}_{n} is the normalized modal displacement vector of the nth POD mode.

The value of mode similarity is between 0 (when the two modes are orthogonal) and 1 (when the two modes are identical). Values closer to 1 represent higher similarity and values closer to 0 lower.

The similarity of M1 of each case to the M1 of its baseline case (π_{11}) is plotted in contour in Fig. 5(a). Three regions can be identified. The first is the region with no or very low CT activation (0-0.1,*). In this region, π_{11} decreased gradually as TA activation level increased but

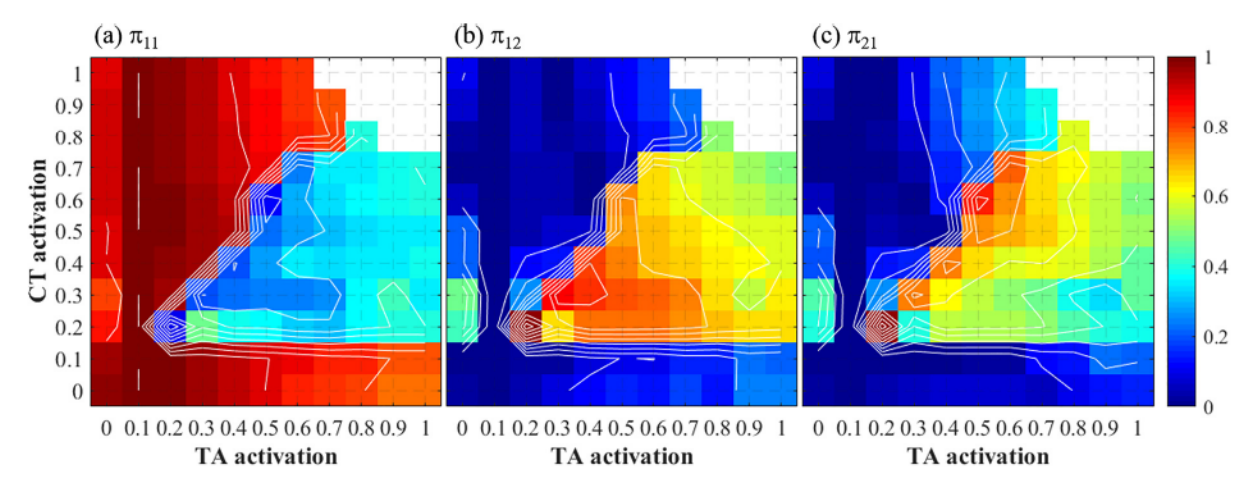


FIG. 5. (Color online) Contours of mode similarity in condition 1 (both the TAv and TAm were active). (a) Similarity between M1 and M1 of (*, 0.1). (b) Similarity between M1 and M2 of (*, 0.1). (c) Similarity between M2 and M1 of (*, 0.1).

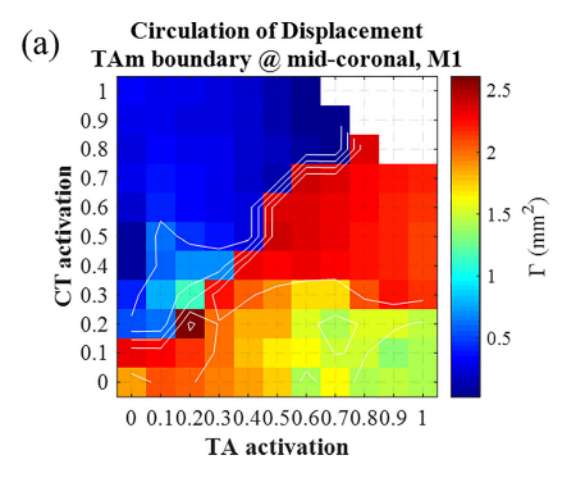
remained above 0.75, indicating that the dominant mode remained the same and no mode change occurred. The second region is the top-left triangular region with CT activation from 0.2 to 1.0. π_{11} was higher than 0.8 in this region. The third region is to the right of the second with higher TA levels. In this region, π_{11} is much lower. The boundary between regions 2 and 3 aligns exactly with where the f_0 drop occurred (shown in Fig. 2). This confirms that a very different mode became the dominant mode after f_0 drop.

To further confirm the mode order switch, mode similarities π_{21} and π_{12} are also computed and plotted [Figs. 5(b) and 5(c)]. π_{21} quantifies the similarity of M2 of each case to M1 of its baseline case, and π_{12} quantifies the similarity of M1 of each case to M2 of the baseline case. The contours of π_{21} and π_{12} both show the same three-region pattern as that in Fig. 5(a), but with the low- and high-value regions swapped. This indicates that M1 and M2 after f_0 drop become highly similar to M2 and M1 of the baseline cases, respectively, confirming the mode order switch for all the cases where the f_0 drop occurred.

Based on the POD mode similarities shown above, M1 in cases (0.5, 0-0.4) and M2 in cases (0.5, 0.5-1.0) can be

regarded as one type of mode and M2 in cases (0.5, 0-0.4) and M1 in cases (0.5, 0.5–1.0) as another type. For ease of discussion, these two types of mode will be termed the lateral mode and the rotational mode based on the main features, specifically. To justify such labelling of the mode shapes, the circulation of the displacement field around the boundary of TAm at the mid-coronal section [see Fig. 1(c)] was calculated as a quantification of rotation in the mode shape. The results are shown in Fig. 6. The contours show the circulation in M1 and M2, respectively. For M1, the modes that are characterized as the lateral modes show nearly zero circulation, whereas the modes that are characterized as the rotational modes show significantly higher circulation. For M2, the division between the two types of modes is not as clear-cut as that in M1, but generally the modes that are characterized as the rotational modes show higher circulation than the modes that are characterized as the lateral modes.

Figure 7 shows the mode energy percentage of the two types of mode for the $a_{\rm CT}\!=\!0.5$ cases. It is clear that a mode transition occurred from $a_{\rm TA}\!=\!0.4$ to $a_{\rm TA}\!=\!0.5$. In this transition, the rotational mode superseded the lateral mode and



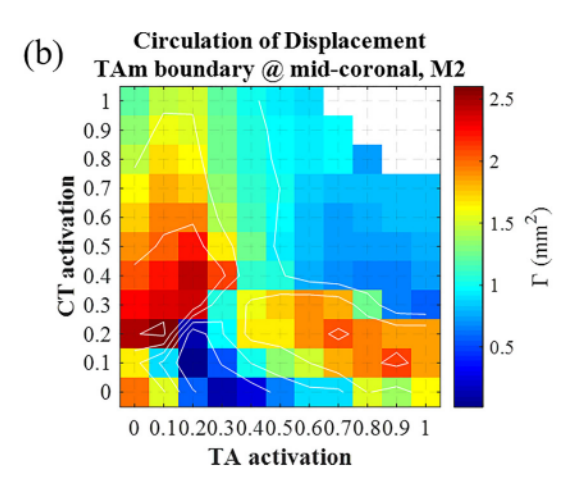


FIG. 6. (Color online) Circulation of the displacement field in the POD modes around the boundary of TAm at mid-coronal section for (a) M1 and (b) M2 in condition 1.

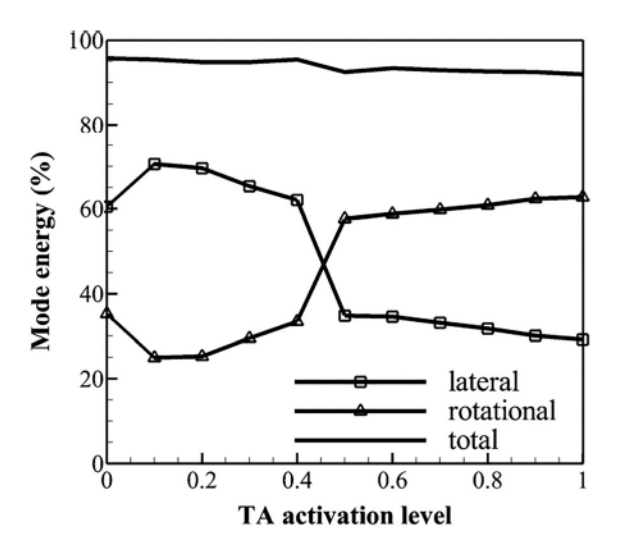


FIG. 7. Mode energy coefficients showing dominant mode switching from lateral to rotational.

became the most dominant mode. It is worth noting that before the mode transition, the energy percentage of the rotational mode also increased with TA activation level and that it increased slightly after the mode switch.

For the lower region where CT activation level is low and TA is very high, higher POD modes were non-negligible as is indicated by the energy contour (Fig. 3). In these cases, more complex modes with cover layer-dominant motion were active. However, since this paper focuses on the non-monotonic f_0 change with TA activity, the detailed vibratory pattern of the vocal fold in this region was not explored.

C. Effects of TAm bundle

In Sec. III B, we demonstrated the mode switch of vocal fold vibration under CT and TA interaction. It can be asked further why the vibratory mode switched with muscle activity and why the mode switch caused frequency drops.

In this section, the effects of the TAm are tested using results from the parametric simulations when only the TAv is active (condition 2). The TAm introduces a nonlinear factor as it stiffens the body while slackening the cover, which promotes a non-homogeneous stress distribution in the body and cover that is likely to cause bifurcation.

The frequency contour of condition 2 is plotted in Fig. 8. The range of f_0 was from 145 Hz at (0, 0) to 193 Hz at (1.0, 1.0), which was close to that of when both the TAv and TAm were active (condition 1). However, f_0 showed a monotonic increase with both CT and TAv activation, and the highest frequency was achieved at the maximum activation of both muscles. At medium TA levels, f_0 was generally lower than in condition 1. Frequency jumps with TA activity only occurred at two locations where the CT level was very low.

The POD analysis was also applied to the cases in condition 2. For condition 2, the total energy percentage of M1 and M2 was above 93% for all the cases. The mode similarity contours are plotted in Fig. 9.

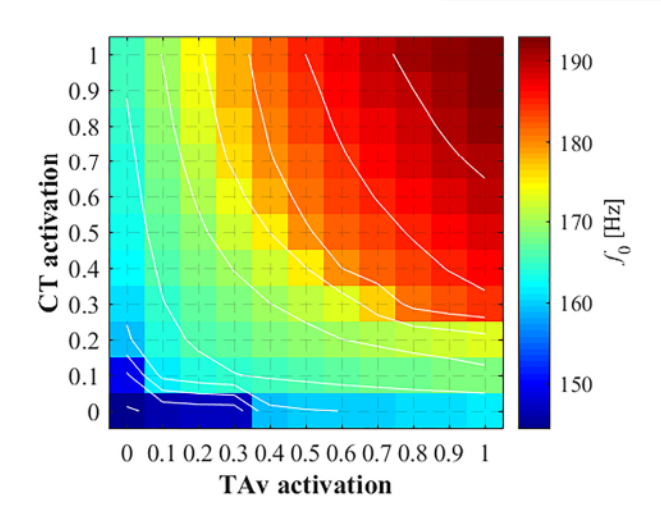


FIG. 8. (Color online) Fundamental frequency variation under CT and TA interaction when only the vocalis muscle was active (condition 2).

From Fig. 9, π_{11} of condition 2 underwent a gradual decrease with TA activity but remained greater than 0.5. Inspection of the mode shapes revealed that M1 had a mode shape similar to that of the lateral mode [M1 of (0.5, 0.4) in condition 1] described in Sec. III B. From Fig. 9(b), π_{22} had a similar pattern except a steeper decrease in the middle region. However, the mode shape of M2 was different from both types described in Sec. III B. No mode order switch occurred in condition 2, as was verified by π_{12} [Fig. 9(c)]. π_{21} (not shown) was similar to π_{12} .

Figure 10 compares the stress in the anterior-posterior (AP) direction (calculated as the volume average of the longitudinal total stress) in the body (TAm) and cover layers and the difference between them for the parametric simulations in conditions 1 and 2. In condition 1, the AP stress in the TAm increased with both CT and TA activities, whereas the AP stress in the cover was largely determined by vocal fold strain. As the AP stress in the TAm was much higher than that in the cover, the AP stress difference was largely determined by the TAm AP stress. In condition 2, as the TAm was not active, AP stress in both TAm and cover was mostly determined by the vocal fold strain. Note that, in both conditions, the AP stress in TAm was always higher than that in the cover layer, indicating that the body layer was stiffer in the current simulation. However, experimental data show that it is possible for the cover layer to have a higher AP stress during vocal fold stretch.²³ Overall, the stress difference between the body and cover layers was much higher when the TAm bundle was active. The AP stress difference increased with both CT and TA activity. The same trend can be inferred from Yin and Zhang.² Note that the contour pattern does not line up with the frequency drop, indicating that it was not the only cause of the mode switch.

IV. DISCUSSION

Previous studies 14,24 have also shown two major types of empirical modes largely accounting for the dynamic

https://doi.org/10.1121/10.0005883

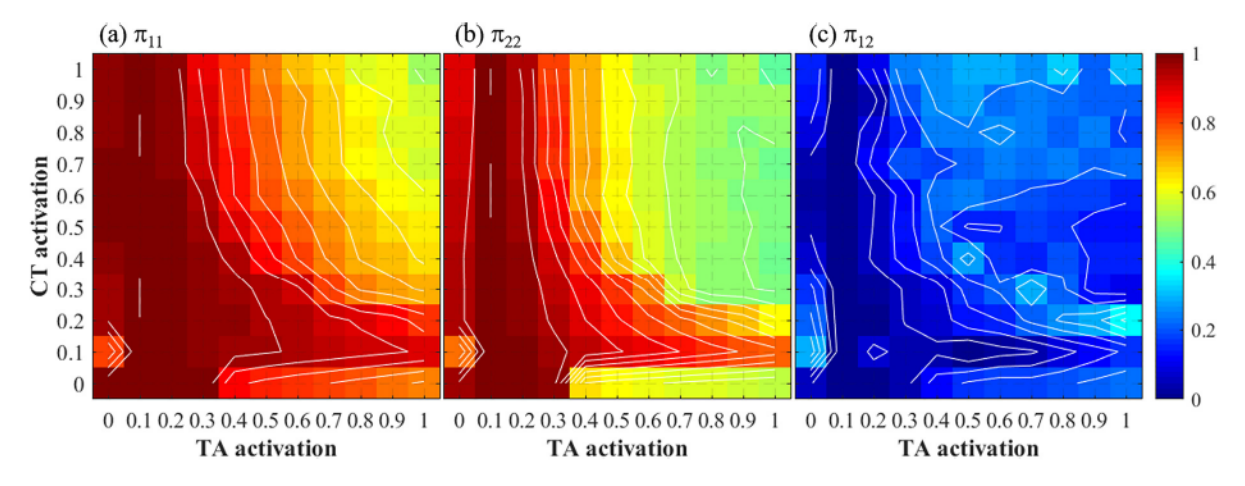


FIG. 9. (Color online) Mode similarities of the first two modes in condition 2. (a) Similarity between M1 and M1 of (*, 0.1). (b) Similarity between M2 and M2 of (*, 0.1). (c) Similarity between M1 and M2 of (*, 0.1).

vibration pattern of the vocal folds. One of them accounts for the lateral movement of the vocal fold, and the other accounts for the alternating divergent/convergent shape change. It appears that either mode could be the more dominant. For example, in the simulation conducted by Alipour and Titze²⁵ and subsequently analyzed by Berry *et al.*, ¹⁴ the convergent/divergent mode was the more dominant. In a later study by Berry *et al.*, ²⁴ where empirical modes were derived from high speed imaging data of vocal fold vibration in excised canine larynges, the lateral mode was found to be the more dominant. Hirano ¹⁰ proposed the body-cover theory of vocal fold vibration and described four different

vocal fold configurations with CT and TA adjustments that enable the vocal fold to vibrate in different patterns. The current results show direct proof that the vocal folds are capable of vibrating in different modes due to changes of muscle activities, which greatly affect the f_0 .

The comparison between the results from conditions 1 and 2 shows that the active stress in the TAm was essential for the mode order switch. It appears that CT activity tends to promote the lateral mode and that TA activity tends to promote the rotational mode. For example, at (0.4, 0.3) in condition 1 (when both the TAv and TAm were active), the lateral mode was dominant. Increasing the TA activation by

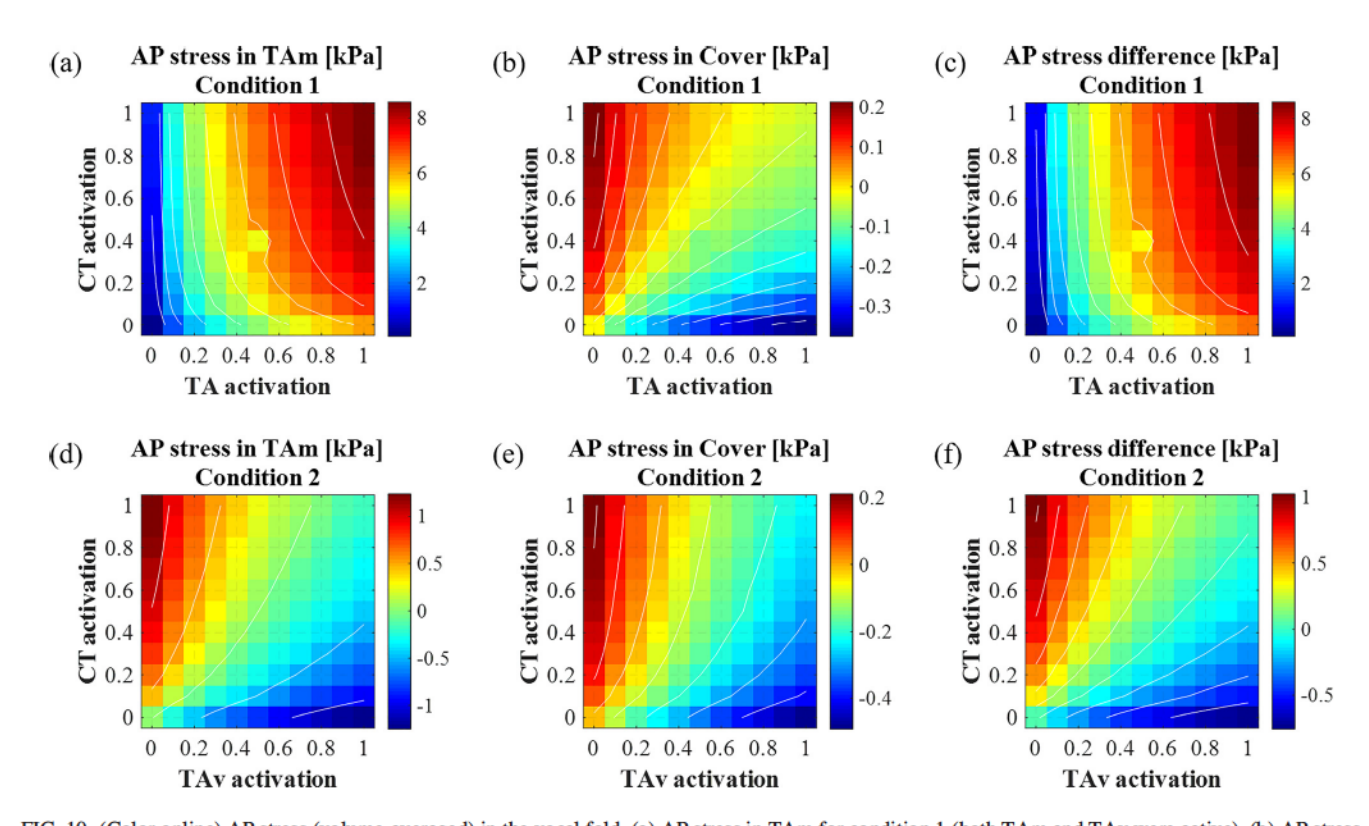


FIG. 10. (Color online) AP stress (volume-averaged) in the vocal fold. (a) AP stress in TAm for condition 1 (both TAm and TAv were active). (b) AP stress in the cover for condition 1. (c) AP stress difference between TAm and the cover for condition 1. (d) AP stress in TAm for condition 2 (only TAv was active). (e) AP stress in the cover for condition 2. (f) AP stress difference between TAm and the cover for condition 2.

10% from here changed the dominant mode to the rotational mode at (0.4, 0.4), from which the dominant mode changed back to the lateral mode when the CT activation was increased by 10% at (0.5, 0.4). These effects of CT and TA on the vibration are likely due to their effects on vocal fold stress distribution. CT stretches both the body and cover, which promotes a homogeneous stress distribution in the vocal fold, making it more likely to vibrate as a singlelayered unit. TA stiffens the body and slackens the cover, which promotes a heterogeneous stress distribution in the vocal fold, making it more likely to vibrate as a two-layered structure. The stiffened body limits the lateral motion of the slackened cover, for which the rotational motion around the stiff core is more easily triggered. From the current simulation results, the mode order switch in condition 1 occurred when the status of cover layer was transitioning between in tension (elongated) and in compression (shortened). This is clear from the stress contour in Fig. 10(b) as the mode transition roughly lined up with the zero AP stress in the cover. However, this does not mean that the mode order switch is associated only with the cover-layer AP stress, because it did not occur in condition 2, where the cover layer was also in compression under high TAv activation.

Titze et al. 1,26 used the concept of effective stiffness and effective vibration depth to explain the role of the TA in controlling f_0 . f_0 is expected to change approximately as the square root of the effective stiffness. How TA activity affects the effective stiffness was thought to depend on how much of the TA is involved in vibration (effective vibration depth; see Titze et al. 26). More specifically, when the vibration is confined to the cover, contraction of TA would lower f_0 due to reduced tension in the cover layer; when the vibration extends deep into the body, TA contraction could increase f_0 if the increased tension in the body layer outweighs the tension decrease in the cover layer. Our results suggested that, besides the vibration depth, vibration mode also affects how TA activity affects the effective stiffness. When the lateral mode was dominant, increasing TA activity increased f_0 , suggesting that the increased TA stress increased the effective stiffness. When the dominant mode switched to the rotational mode, f_0 underwent an abrupt drop. Moreover, after that, when the rotational mode became dominant, increasing TA activity only slightly increased f_0 . Note that the vibration amplitudes of the TA in both modes were close. These results suggested that the rotational mode reduced the contribution of TA stress to the effective stress. Therefore, vibration mode can play an important role in muscle regulation of f_0 by affecting the contribution of muscle stress to the effective stiffness.

The increase in f_0 with TA activity even under high CT activation shows that a low to medium level of TA activation is important in achieving high pitch in phonation. McCulloch *et al.*²⁷ showed that higher pitch generally involved higher TA activity in an EMG study. While the common belief is that the falsetto register is CT-dominant with little or no TA activity (see, e.g., Hirano^{5,10}), Hull⁷ reported from EMG investigation that TA level also

increased as pitch rose in most of the subjects, and TA activity could be higher in the falsetto than in the chest register in some subjects. In the in vivo results reported by Chhetri et al., only two data points were in the falsetto region $(f_0 >$ 400 Hz) when TA was not activated. Chhetri and Park summarized in another in vivo study that in the higher register f_0 is controlled by both CT and TA.²⁸ The average passive stress of the human vocal ligament tissue under full elongation is around 50 kPa, ^{23,29} which is on par with the active stress of the TA with medium activation (note that the maximum active stress of the TA is around 100 kPa³⁰). This seems to indicate that the active stress in the TA layer could function synergistically to the tension in the ligament to increase f_0 , because the proximity in AP stress in the different layers increases the homogeneity of the structure, making it more likely to function as a single vibratory unit.

The optimal stretch of vocal fold muscles is greater than one,^{30,31} that is, the maximum possible active stress is achieved under elongation. In the several models of the laryngeal muscles, 2,17 this value is between 1.2 and 1.5. This has implications for the role of CT in frequency regulation. CT is commonly thought to stretch the vocal fold to increase the tension in the ligament to increase the frequency. The often overlooked part is that it also increases the active stress in the TA by making it closer to the optimal stretch. This effect is stronger when TA activity is higher. A more effective strategy to increase the AP stress in the vocal fold is to have higher CT activation than the TA so that the vocal fold is elongated and the active stress of TA is higher due to it being closer to the optimum stress. This seems more effective than a higher-TA-than-CT strategy, in which case the tension in the cover layer would be lower. It is worth noting that TAs are usually activated up to medium levels during normal phonation and full activation of TA is typically seen in non-phonatory activities such as swallowing.

The f_0 of the human voice is a very important factor affecting its perception. The ability to modulate frequency is vital in communication. For example, for a typical natural sounding English phrase, the f_0 can vary by 1.7 times (e.g., in Story³²), or about 9 semitones. However, the muscle activity related to the frequency variation in speech and singing appears not to be uniform across subjects^{6,7} and is affected by vocal training.33 Different pathways also seem possible even within the same register. For example, in the in vivo experiment by Chhetri et al., an f_0 of approximately 550 Hz can be achieved either with CT level 86% and TA 25% or with CT 71% and TA level 50%, both of which lie in the falsetto regime judging by f_0 . The current simulation also showed the possibility of achieving the same frequency with different muscle activities under the same vibratory pattern. Further investigation is needed to compare the characteristics of the different pathways of f_0 control.

Finally, it is worth mentioning some of the limitations of the current study. The simulated frequency range was limited, mostly due to uncertainty in material properties and limited vocal fold stretch in the current model, which was subject-specific and canine-based and did not include the

ligament. The separation of the TAm and TAv, which is challenging even in anatomical dissection,³⁴ is prone to high uncertainty, because the boundary between them is not clear in the MRI scan. Moreover, the model was based on an artificially adducted larynx; thus, the TA's effect on vocal fold adduction could be different from that in vocal folds from a natural neutral position. The LCA was not active in the simulation. As a result, the level of adduction, which also has an impact on the vocal fold dynamics, was largely fixed. For the muscle model, the dependence of active stress on strain rate and local fiber orientation was not considered. Since steady-state vocal fold vibration was the focus, the effect of muscle active stress dependence on strain rate is expected to be small. The use of single global orientation for all elements in a muscle bundle might be justifiable since the muscle fibers of the TA (especially the TAv) mostly run in parallel in the longitudinal direction. However, the change of local fiber orientation with vocal fold deformation during vibration could also affect the vocal fold dynamics. Its effect needs to be investigated in the future. The current discussion focused on the internal stresses of the vocal fold without paying attention to other important factors such as the geometry, in plane stiffness, level of adduction, and subglottal pressure. For example, Jiang et al. 35 reported bifurcation in vocal fold dynamics with gradual modification of coverlayer geometry. Needless to say, subglottal pressure is another important factor in determining the vibration mode. In the current study, a fixed subglottal pressure of 2kPa was used, which was higher than the onset pressure under most activation conditions.³ We expect that, if broad subglottic pressures were to be included, different vibration modes might be observed, and the bifurcation of vibration modes might occur at different muscle activation levels. Last, while previous studies have shown that 1D flow models are adequate in predicting the qualitative vocal fold vibration, its interaction with muscle activation has not been investigated. The exact boundary where the frequency jumps occurred might have been different if higher-order flow models had been used.

V. CONCLUSION

Using a MRI-based continuum model with simulated muscle activity, parametric FSI simulations were conducted to investigate the effects of interaction of CT and TA on vocal fold dynamics. Under medium to high CT activation, f_0 first increased with TA activity and then underwent a downward jump, after which it remained low regardless of TA activity. Such a trend was also reported in an *in vivo* experiment.³ POD analysis revealed that the vocal fold vibrations were dominated by two modes representing a lateral motion and rotational motion, respectively, and the f_0 drop was associated with a switch of the order of the two modes. In another parametric set where only the vocalis was active, f_0 increased monotonically with both TA and CT activity and the mode switch did not occur. The results suggested that the active stress in the TA, which causes large

stress differences between the body and cover, is essential for the occurrence of the rotational mode and mode switch. Relatively greater TA activity tends to promote the rotational mode, while relatively greater CT activity tends to promote the lateral mode. The results also suggested that vibration mode plays an important role in muscle regulation of f_0 by affecting the contribution of muscle stress to the effective stiffness. In our results, the rotational mode reduced the contribution of the TA stress to the effective stiffness, causing the downward jump and afterward slow increase in f_0 with increased TA activity after the dominant mode switched from lateral to rotational.

ACKNOWLEDGMENTS

This study is supported by the National Science Foundation under Grant 245 No. 1652632. The numerical simulation was supported by the Extreme Science and Engineering Discovery Environment (XSEDE) under Allocation Award No. TG-CTS180004. The open source finite element package CalculiX³⁶ was used for the simulations in this study.

APPENDIX: DETAILS OF MUSCLE MODEL

The passive material properties of the muscle tissue were modeled using fiber-reinforced materials. The active stress was modeled using contractile elements based on the Hill model. The implementation and validation of the muscle model were reported in our previous work. ¹⁶ The passive strain energy is defined as

$$U = C_{10}(\bar{I}_1 - 3) + \frac{1}{D_1}(J - 1)^2 + \frac{k_1}{2k_2} \left[e^{k_2(\bar{I}_4 - 1)^2} - 1 \right],$$
(A1)

where \bar{I}_1 and \bar{I}_4 are the first and the fourth invariant of the reduced Cauchy–Green tensor, respectively, J is the Jacobian determinant of the deformation, C_{10} is the isotropic neo-Hookean parameter, k_1 is a modulus-like parameter, k_2 is a dimensionless parameter, which accounts for the degree of nonlinearity, and D_1 is the compressibility factor, which was set to a value close to zero $[1/(20C_{10})]$ to approximate the incompressibility of vocal fold tissues. The relationship between the stress tensor and the deformation for this strain energy function can be obtained by taking the derivative of the strain energy function with respect to the right Cauchy–Green tensor as³⁷

$$S_{KL} = 2C_{10} \frac{\partial \overline{I}_1}{\partial C_{KL}} + \frac{2}{D_1} \left(1 - \frac{1}{\sqrt{I_3}} \right) \frac{\partial I_3}{\partial C_{KL}}$$

$$+ 2k_1 (\overline{I}_4 - 1) e^{k_2 (\overline{I}_4 - 1)^2} \frac{\partial \overline{I}_4}{\partial C_{KL}}, \tag{A2}$$

where K and L are the subscript for indicial notation, S_{KL} is the second Piola–Kirchhoff stress tensor, and I_3 is the third invariant of the right Cauchy–Green deformation tensor C_{KL} .

The Hill-based contractile model for active stress is formulated as

$$\sigma_A = a(t)\sigma_{\max}\sigma_{TL}^*\sigma_{TV}^*,\tag{A3}$$

where σ_A is the active stress, a(t) is the activation level, σ_{\max} is the maximum active muscle stress, and σ_{TL}^* and σ_{TL}^* are scaling factors as functions of muscle stretch and stretch rate, respectively. σ_{TL}^* is formulated as

$$\sigma_{TL}^* = \exp\left[-\left(\frac{\lambda - \lambda_{opt}}{s_f}\right)^2\right] + m\lambda,$$
 (A4)

where λ is the stretch ratio of the muscle, defined as the current length over the initial length and thus deformation dependent. λ_{opt} is the optimal stretch ratio, at which maximum stress is achieved. In addition to that, the shape factor s_f and the slope parameter m control the shape and asymmetry of the relation. λ_{opt} , s_f , and m were set to 1.5, 0.35, and 0.01, respectively. ^{16,17} The dependence of the active stress on stretch rate was not considered. The value of σ_{TV}^* was set to 1 as a constant.

Material parameters for the muscle tissues (listed in Table II) were the same as those used in the previous study, 15 which were determined by curve fitting experimental data of canine tissues in uniaxial stretch. The curve fitting for the passive parameters of the CT and TA muscles was described in a previous work 16 using experimental measurements.30,31 Note that the same parameters were used for CT and TA because they have almost identical passive response.³⁸ Passive parameters for the other muscles [LCA, interarytenoid (IA), and posterior cricoarytenoid (PCA)] were obtained in a similar way based on experimental data. 38 The maximum active stresses of the canine laryngeal muscles were measured extensively by Alipour-Haghighi et al.;30,31,39 CT and TA both have a maximum active stress around 100 kPa. The other muscles (IA, LCA, and PCA) seem to have lower maximum active stress, 40 but the authors mentioned that it could be due to the samples being not as fresh. Previous models^{41,42} have also assumed for these muscles the same maximum active stress as that of TA. However, the maximum active stress of the IA, LCA, and PCA muscles does not affect the current simulations since they were not active.

The muscle model was implemented in the open source finite element software CalculiX.³⁶ The uniaxial active stress computed using Eq. (A3) was transformed into a

TABLE II. Material parameters for muscle tissues.

Muscle	C ₁₀ (kPa)	k_1 (kPa)	k_2	σ _{max} (kPa)
TAv	3	0.15	9	100
TAm	3	0.15	9	80
CT (all bellies)	3	0.15	9	100
Lateral cricoarytenoid	2.7	2	5.5	100
Posterior cricoarytenoid (all bellies)	2.7	2	5.5	100
Interarytenoid	2.035	10	2.5	200

stress tensor based on the muscle orientation and then added to the passive stress as the total stress that satisfies the equilibrium.

- ¹I. R. Titze, E. S. Luschei, and M. Hirano, "Role of the thyroarytenoid muscle in regulation of fundamental frequency," J. Voice 3, 213–224 (1989).
- ²J. Yin and Z. Zhang, "The influence of thyroarytenoid and cricothyroid muscle activation on vocal fold stiffness and eigenfrequencies," Proc. Meet. Acoust. 133, 2972–2983 (2013).
- ³D. K. Chhetri, J. Neubauer, E. Sofer, and D. A. Berry, "Influence and interactions of laryngeal adductors and cricothyroid muscles on fundamental frequency and glottal posture control," J. Acoust. Soc. Am. 135, 2052–2064 (2014).
- ⁴A. Peckham, *The Contemporary Singer: Elements of Vocal Technique* (Berklee, Boston, MA, 2010).
- ⁵M. Hirano, "Vocal mechanisms in singing: Laryngological and phoniatric aspects," J. Voice 2, 51–69 (1988).
- ⁶K. A. Kochis-Jennings, E. M. Finnegan, H. T. Hoffman, S. Jaiswal, and D. Hull, "Cricothyroid muscle and thyroarytenoid muscle dominance in vocal register control: Preliminary results," J. Voice 28, 652.e21–652.e29 (2014).
- ⁷D. M. Hull, "Thyroarytenoid and cricothyroid muscular activity in vocal register control," Master thesis, University of Iowa, Iowa City, IA (2013).
 ⁸N. Henrich, "Mirroring the voice from Garcia to the present day: Some insights into singing voice registers," Logoped. Phoniatr. Vocol. 31, 3–14 (2006).
- ⁹J. G. Svec, J. Sundberg, and S. Hertegard, "Chest, head and whistle registers in an untrained female singer analyzed by videokymography, strobolaryngoscopy and sound spectrography," J. Acoust. Soc. Am. 123, 3243–3243 (2008).
- ¹⁰M. Hirano, "Morphological structure of the vocal cord as a vibrator and its variations," Folia Phoniatr. Logop. 26, 89–94 (1974).
- ¹¹S. Saito, H. Fukuda, S. Kitahara, Y. Isogai, T. Tsuzuld, H. Muta, B. Thkayama, T. Fujioka, N. Kokawa, and K. Makino, "Pellet tracking in the vocal fold while phonating: Experimental study using canine larynges with muscle activity," in *Vocal Fold Physiology: Biomechanics, Acoustics and Phonatory Control*, edited by I. R. Titze and R. C. Scherer (Denver Center for the Performing Arts, Denver, CO), pp. 169–182 (1985).
- ¹²J. G. Svec, H. K. Schutte, and D. G. Miller, "On pitch jumps between chest and falsetto registers in voice: Data from living and excised human larynges," J. Acoust. Soc. Am. 106, 1523–1531 (1999).
- ¹³T.-Y. Hsiao, C.-M. Liu, C.-J. Hsu, S.-Y. Lee, and K.-N. Lin, "Inducing vocal register transition in an *in vivo* evoked phonation canine model," J. Formos. Med. Assoc. **100**, 543–547 (2001).
- ¹⁴D. A. Berry, H. Herzel, I. R. Titze, and K. Krischer, "Interpretation of biomechanical simulations of normal and chaotic vocal fold oscillations with empirical eigenfunctions," J. Acoust. Soc. Am. 95, 3595–3604 (1994).
- ¹⁵B. Geng, N. Pham, Q. Xue, and X. Zheng, "A three-dimensional vocal fold posturing model based on muscle mechanics and magnetic resonance imaging of a canine larynx," J. Acoust. Soc. Am. 147, 2597–2608 (2020).
- ¹⁶N. Pham, Q. Xue, and X. Zheng, "Coupling between a fiber-reinforced model and a Hill-based contractile model for passive and active tissue properties of laryngeal muscles: A finite element study," J. Acoust. Soc. Am. 144, EL248–EL253 (2018).
- ¹⁷S. L. Smith and E. J. Hunter, "A viscoelastic laryngeal muscle model with active components," J. Acoust. Soc. Am. 135, 2041–2051 (2014).
- ¹⁸G. Z. Decker and S. L. Thomson, "Computational simulations of vocal fold vibration: Bernoulli versus Navier–Stokes," J. Voice 21, 273–284 (2007).
- ¹⁹J. J. Jiang and I. R. Titze, "Measurement of vocal fold intraglottal pressure and impact stress," J. Voice 8, 132–144 (1994).
- ²⁰A. Chatterjee, "An introduction to the proper orthogonal decomposition," Curr. Sci. 78, 808–817 (2000).
- ²¹S. Yin, Y. Fan, M. Sandberg, and Y. Li, "PIV based POD analysis of coherent structures in flow patterns generated by triple interacting buoyant plumes," Build. Environ. 158, 165–181 (2019).
- ²²D. K. Chhetri, J. Neubauer, and D. A. Berry, "Neuromuscular control of fundamental frequency and glottal posture at phonation onset," J. Acoust. Soc. Am. 131, 1401–1412 (2012).

JASA

https://doi.org/10.1121/10.0005883

- ²³Y. B. Min, I. R. Titze, and F. Alipour-Haghighi, "Stress-strain response of the human vocal ligament," Ann. Otol. Rhinol. Laryngol. 104, 563–569 (1995).
- ²⁴D. A. Berry, D. W. Montequin, and N. Tayama, "High-speed digital imaging of the medial surface of the vocal folds," J. Acoust. Soc. Am. 110, 2539–2547 (2001).
- ²⁵F. Alipour-Haghighi and I. R. Titze, "Simulation of particle trajectories of vocal fold tissue during phonation," in *Vocal Fold Physiology: Biomechanics, Acoustics and Phonatory Control*, edited by I. R. Titze and R. C. Scherer (Denver Center for the Performing Arts, Denver, CO), pp. 183–190 (1983).
- ²⁶I. R. Titze, J. Jiang, and D. G. Drucker, "Preliminaries to the body-cover theory of pitch control," J. Voice 1, 314–319 (1988).
- ²⁷T. M. McCulloch, A. L. Perlman, P. M. Palmer, and D. J. Van Daele, "Laryngeal activity during swallow, phonation, and the Valsalva maneuver: An electromyographic analysis," Laryngoscope 106, 1351–1358 (1996).
- ²⁸D. K. Chhetri and S. J. Park, "Interactions of subglottal pressure and neuromuscular activation on fundamental frequency and intensity," Laryngoscope 126, 1123–1130 (2016).
- ²⁹K. Zhang, T. Siegmund, R. W. Chan, and M. Fu, "Predictions of fundamental frequency changes during phonation based on a biomechanical model of the vocal fold lamina propria," J. Voice 23, 277–282 (2009).
- ³⁰F. Alipour-Haghighi, I. R. Titze, and A. L. Perlman, "Tetanic contraction in vocal fold muscle," J. Speech Lang. Hear. Res. 32, 226–231 (1989).
- ³¹F. Alipour-Hachichi, A. L. Perlman, and I. R. Titze, "Tetanic response of the cricothyroid muscle," Ann. Otol. Rhinol. Laryngol. 100, 626–631 (1991).
- ³²B. H. Story, "Phrase-level speech simulation with an airway modulation model of speech production," Comput. Speech Lang. 27, 989–1010 (2013).

- ³³K. A. Kochis-Jennings, E. M. Finnegan, H. T. Hoffman, and S. Jaiswal, "Laryngeal muscle activity and vocal fold adduction during chest, chest-mix, headmix, and head registers in females," J. Voice 26, 182–193 (2012).
- ³⁴F. Alipour, K. A. Cox, and I. R. Titze, "Geometric structure of the human and canine cricothyroid and thyroarytenoid muscles for biomechanical applications," Ann. Otol. Rhinol. Laryngol. 108, 1151–1158 (1999).
- ³⁵W. Jiang, X. Zheng, and Q. Xue, "Influence of vocal fold cover layer thickness on its vibratory dynamics during voice production," J. Acoust. Soc. Am. 146, 369–380 (2019).
- ³⁶G. Dhondt and K. Wittig, "A free software three-dimensional structural finite element program" (1998), www.calculix.de (Last viewed May 18, 2021)
- ³⁷G. Dhondt, The Finite Element Method for Three-Dimensional Thermomechanical Applications (John Wiley & Sons, Chichester, UK, 2004), pp. 219–223.
- ³⁸E. J. Hunter and I. R. Titze, "Refinements in modeling the passive properties of laryngeal soft tissue," J. Appl. Physiol. 103, 206–219 (2007).
- ³⁹F. Alipour and I. Titze, "Active and passive characteristics of the canine cricothyroid muscles," J. Voice 13, 1–10 (1999).
- ⁴⁰F. Alipour, I. R. Titze, E. Hunter, and N. Tayama, "Active and passive properties of canine abduction/adduction laryngeal muscles," J. Voice 19, 350–359 (2005).
- ⁴¹E. J. Hunter, I. R. Titze, and F. Alipour, "A three-dimensional model of vocal fold abduction/adduction," J. Acoust. Soc. Am. 115, 1747–1759 (2004).
- ⁴²J. Yin and Z. Zhang, "Laryngeal muscular control of vocal fold posturing: Numerical modeling and experimental validation," J. Acoust. Soc. Am. 140, EL280–EL284 (2016).